Rev.Adv.Mater.Sci. 7 (2004) 1-12

MICROSTRUCTURAL DEVELOPMENTS IN A SPRAY-CAST Al-7034 ALLOY PROCESSED BY EQUAL-CHANNEL ANGULAR PRESSING

Marco J. Starink[1], Nong Gao[1], Minoru Furukawa[2], Zenji Horita[3], Cheng Xu[4] and Terence G. Langdon[4]

[1]Materials Research Group, School of Engineering Sciences University of Southampton, Southampton SO17 1BJ, U.K.
[2]Department of Technology, Fukuoka University of Education Munakata, Fukuoka 811-4192, Japan
[3]Department of Materials Science and Engineering, Faculty of Engineering Kyushu University, Fukuoka 812-8581, Japan
[4]Departments of Aerospace & Mechanical Engineering and Materials Science, University of Southern California, Los Angeles, CA 90089-1453, USA

Received: April 12, 2004

Abstract. A spray-cast Al-7034 alloy was processed by equal-channel angular pressing (ECAP) to produce an ultrafine submicrometer grain size. The microstructures of the as-received and as-pressed alloy were examined using several different experimental techniques including transmission electron microscopy (TEM), electron back-scatter diffraction (EBSD) and differential scanning calorimetry (DSC). The alloy contains η phase ($MgZn_2$) and Al_3Zr precipitates and these precipitates serve to inhibit grain growth so that an ultrafine submicrometer grain size is retained at temperatures up to and above 600K. The results demonstrate an increase in the fraction of high-angle boundaries with increasing numbers of passes in ECAP and analysis of the DSC curves leads to the identification of several thermal effects involving the formation, coarsening and dissolution of the η-phase. The rod-like η-phase particles present in the as-received alloy are broken during ECAP and a detailed analysis suggests this breaking occurs primarily in the first pass of ECAP. Tensile tests at elevated temperature demonstrate a potential for achieving superplastic elongations in the as-pressed material.

1. INTRODUCTION

Severe plastic deformation (SPD) is a processing technique that has received considerable attention over the last ten years [1-5]. The basic principle of SPD processing is that a very high strain is introduced into a material without any concomitant reduction in the cross-sectional dimensions of the work-piece. Thus, SPD processing is different from all conventional industrial procedures such as extrusion, rolling and drawing.

Several different methods are now available for performing SPD processing but most attention has been devoted to date to the two techniques of Equal-Channel Angular Pressing (ECAP) and High-Pressure Torsion (HPT). In ECAP, a rod or bar sample is pressed through a die constrained within a channel that is bent through an abrupt angle within the die. Typically, ECAP is conducted where the angle between the two parts of the channel is 90°. In HPT, a small disk, typically having a diameter of ~1 cm and a thickness of ~0.5-0.8 mm, is subjected to a high pressure and concurrent torsional straining. Both techniques are very effective in leading to the introduction of extremely high strains but in practice ECAP is a more viable technique because it can be scaled up relatively easily to produce fairly large bulk samples [6].

The potential for processing by ECAP was first proposed over two decades ago by Segal and coworkers [7] and subsequently there have been nu-

Corresponding author: Marco J. Starink, e-mail: m.j.starink@soton.ac.uk

merous reports summarizing the principles and practices of ECAP [8-11]. It was recognized over ten years ago that ECAP is a remarkably effective procedure for producing metallic alloys with ultrafine grain sizes [12,13] where these grain sizes are typically in the submicrometer range but occasionally they may lie within the nanometer range. Thus, the increasing current interest in the fabrication, properties and utilization of nanostructured and ultrafine-grained materials has prompted an ever-growing interest in the use of ECAP as a processing tool.

In principle, two advantages may be gained by using ECAP to refine the grain size to the submicrometer level. First, the strength will increase at ambient temperatures through the Hall-Petch relationship [14,15]. Second, if an ultrafine grain size is retained to reasonably high temperatures where diffusion-controlled processes become rapid, there is a potential for introducing a superplastic forming capability into metallic alloys even when they are not inherently superplastic. Furthermore, it was noted in an early report that a superplastic regime should occur in ultrafine-grained materials at faster strain rates and at lower temperatures by comparison with conventional superplastic forming operations where the grain sizes are typically an order of magnitude larger at ~2-5 μm [16]. Both of these changes are attractive for the superplastic forming industry because faster strain rates lead to shorter forming times and lower operating temperatures reduce the problems associated with tool wear.

Numerous investigations have now established that the ultrafine grains introduced through ECAP may be retained to reasonably high temperatures provided the alloy contains a fairly uniform dispersion of precipitates which serve to restrict grain growth at elevated temperatures [17-21]. Most experiments to date have been conducted using conventional cast alloys. However, it is reasonable to anticipate that spray-casting may be especially effective in producing superplastic alloys because it is well established that spray-casting produces a higher density of dispersed particles than in conventional cast alloys [22,23]. In spray-casting, an atomised molten metal is spray deposited at high velocity using an inert gas and this yields a fully-dense material with a reasonably small grain size. Experiments showed that the ECAP processing of an Al-5091 Al-Mg-Li alloy containing $Al_3(Zr,Ti)$ dispersoids produced an ultrafine grain size of ~0.3-0.6 μm and, in addition, there was reasonable stability of these very small grains up to temperatures of the order of 673K [23]. Very recently, experiments were conducted to evaluate the potential for using ECAP to attain superplastic ductilities in a spray-cast Al-7034 Al-Zn-Mg-Cu alloy [24,25] and these tests will form the background for this detailed report.

It is well established that the 7xxx-type alloys can be precipitation hardened and, in general, there are two precipitation processes occurring in Al-Zn-Mg-Cu alloys having a low content of Cu [26,27]:

$$\alpha_{ss} \rightarrow \text{GP zones} \rightarrow \eta' \rightarrow \eta\ ,$$

$$\alpha_{ss} \rightarrow T\ .$$

In these reactions, α_{ss} is the supersaturated solid solution, GP represents the Guinier-Preston zones, η' is a metastable phase and η and T are the equilibrium phases. The η-phase is a quaternary phase containing Al, Zn, Mg and Cu and it is based on a solid solution of $MgZn_2$ with AlCuMg components (for example, $Mg(Zn,Al,Mg)_2$ or $Mg(Zn_2,AlMg)$) [28,29] and the T-phase is a quaternary phase based on $Mg_3Zn_3Al_2$. In most alloys, there is a general tendency for the η precipitation sequence to dominate. Among these phases, the η'-phase and the η-phase are the primary strengthening precipitates in peak aged (T6) and overaged (T7) 7xxx-series alloys.

In 7xxx alloys subjected to thermo-mechanical processing, the grain structure is controlled primarily by the η-phase and by the presence of dispersoid particles formed through the addition of Cr, Zr and/or Sc. In the present ECAP experiments on a spray-cast Al-7034 alloy, grain refinement is aided by the presence of a very fine dispersion of Al_3Zr precipitates which were formed as a consequence of the addition of 0.2% Zr.

The purpose of this paper is to review recent experimental work on microstructural evolution in the Al-7034 alloy processed by ECAP and to present new data obtained using differential scanning calorimetry (DSC) and electron back-scatter diffraction (EBSD) analysis.

2. EXPERIMENTAL MATERIAL AND PROCEDURES

All of the experiments were conducted using a spray-cast Al-7034 alloy produced commercially by Osprey Metals, Ltd. (Neath, U.K.). The as-received alloy was chemically analyzed to reveal the following composition (in wt.%): 11.5% Zn, 2.5% Mg, 0.9% Cu and 0.20% Zr with the balance as Al. The material was produced in the form of an ingot with a diameter of 356 mm. It was then extruded using an extrusion ratio of 35 to give a rod having a diameter of 63.5

mm. This rod was homogenized for 16 h at 733K, air cooled and then extruded using an extrusion ratio of 50 in a single pass to give several rods having diameters of 9.5 mm. Each rod was cut into a series of billets having lengths of 64 mm. These billets were subjected to the ECAP processing.

A solid die was used for ECAP with an internal angle of $\Phi = 90°$ between the two parts of the channel and an outer arc of curvature of $\Psi = 20°$ at the intersection of these two parts. It can be shown from first principles that these values of Φ and Ψ lead to an imposed strain close to ~1 on each passage of the billet through the die [30]. In the present experiments, the same billets were pressed repetitively up to a total of 8 passes in order to achieve strains up to ~8. All of the processing was conducted at a temperature of 473K using route B_C in which the samples are rotated by 90° in the same sense between each pass [31].

In order to evaluate the potential for achieving superplasticity in this alloy, tensile specimens were machined from both the as-received alloy and the alloy after processing by ECAP. These specimens were cut with their gauge lengths parallel to the longitudinal axes of the billets and with gauge lengths of 4 mm and cross-sectional areas of 3×2 mm^2. All tensile specimens were pulled to failure at temperatures in the range from 573 to 698K using a testing machine operating at a constant rate of cross-head displacement and with initial strain rates from 1.0×10^{-3} to 1.0×10^{-1} s^{-1}.

The value of the melting temperature of the as-received alloy was evaluated by differential scanning calorimetry (DSC) using a MacScience DSC3300S calorimeter and a pure Al standard. Through the heating of a sample at a rate of 10 K min^{-1} in an argon atmosphere, the incipient melting temperature was estimated as ~798K. Additional DSC experiments were performed with a Perkin-Elmer Pyris 1 calorimeter using a nitrogen atmosphere, a constant heating rate of 10 K·min^{-1} and with the samples in the form of discs having diameters and thicknesses of ~5.0 mm and ~0.9 mm, respectively. All of the DSC runs were corrected by subtracting the DSC baseline obtained from a run with an empty pan. For additional baseline corrections, to compensate for the heat capacity differences and apparatus imperfections giving short-term and long-term baseline drifts, a second-order polynomial function was subtracted from the measured heat flows. The parameters for this second-order polynomial function were fitted by taking the heat flow to reactions as zero at the three temperatures of 353, 453, and 793K.

All of the electron backscatter diffraction (EBSD) analysis was performed using a JEOL JSM-6500 high-performance FEG-SEM employing an individual step size of 0.05 mm and the EBSD data were analyzed using HKL Channel 5 software. The nature of the microstructure was examined using an Hitachi H-8100 transmission electron microscope (TEM) operating at 200 kV. For samples subjected to ECAP, the TEM observations were performed on the flow or Y plane equivalent to the side face at the point of exit from the ECAP die. Selected area electron diffraction (SAED) patterns were taken in the TEM using aperture sizes of 12.3 or 2.5 μm.

3. EXPERIMENTAL RESULTS

The application of ECAP processing introduces an exceptionally high density of dislocations into the deformed billet and this is accompanied by various concomitant microstructural changes in the alloy. In order to obtain detailed information on these changes, it is necessary to make use of a range of sophisticated investigative techniques. In this study, the microstructure of the spray-cast Al-7034 alloy was interpreted using detailed information obtained from DSC analysis and from TEM, EBSD and optical microscopy.

3.1. Microstructural characteristics

The appearance of the as-received alloy in TEM is shown in Figs. 1a and 1b at two different magnifications: the associated SAED patterns were taken using aperture sizes of 12.3 and 2.5 μm, respectively. An important characteristic of the as-received microstructure is the presence of fairly large rod-like η-phase ($MgZn_2$) precipitates which are clearly visible in Fig. 1b. Inspection showed these precipitates were distributed reasonably homogeneously throughout the alloy and measurements gave average lengths of ~0.5 μm and average widths of ~0.07 μm. In addition, there was a very fine dispersion of Al_3Zr precipitates in the alloy as revealed by the presence of $L1_2$ superlattice spots in the SAED patterns. The grain configuration in the as-received condition was essentially equiaxed with a measured average grain size of ~2.1 μm and with a fairly low density of dislocations lying within the grains.

Figs. 2a and 2b show TEM micrographs of the microstructure at two different magnifications after processing by ECAP through six passes at 473K so that the total imposed strain is ~6. It is important to note from Fig. 2b that the rod-like η-phase precipitates are no longer visible after ECAP to a

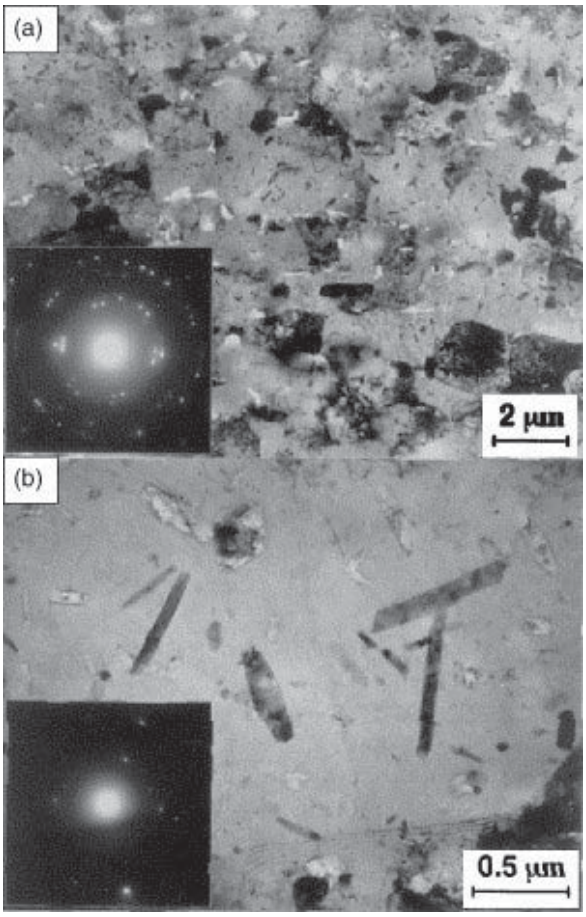

Fig.1. Microstructure in the as-received Al-7034 alloy at (a) low and (b) high magnifications: the SAED patterns were recorded using aperture sizes of 12.3 and 2.5 μm, respectively.

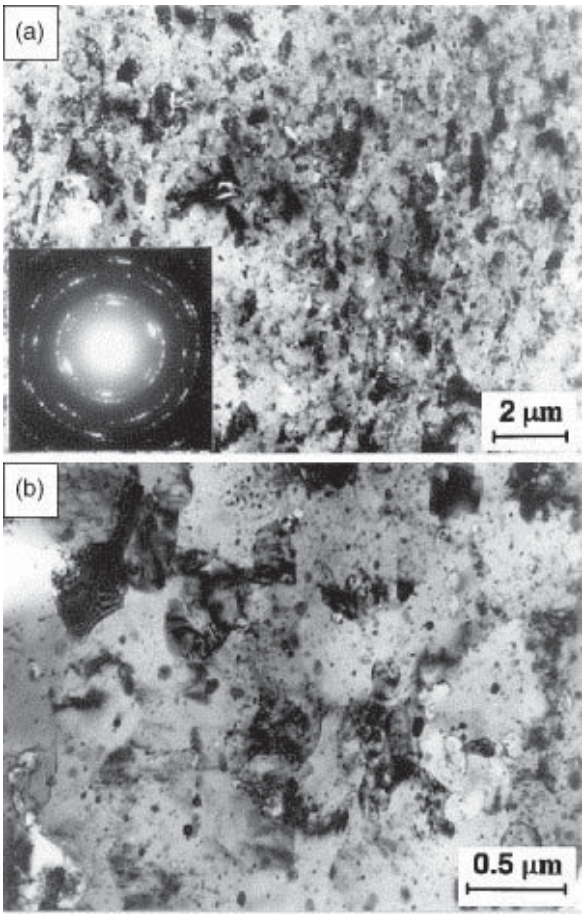

Fig. 2. Microstructure after ECAP through 6 passes at 473K at (a) low and (b) high magnifications: the SAED pattern was recorded using an aperture size of 12.3 μm.

strain of ~6 and it is therefore concluded that the high stresses imposed during ECAP are sufficient to break the rod-like precipitates into smaller fragments. The occurrence of precipitate fragmentation during ECAP has been reported also in other earlier investigations of Al-based alloys [32-34]. As anticipated, the grain size was significantly reduced by ECAP processing: the grain size in Fig. 2a was measured as ~0.3 μm and the SAED pattern suggests the presence of a large fraction of boundaries having high angles of misorientation.

3.2 Analysis of the DSC curves

Fig. 3 shows the DSC thermograms (a) over the entire range of temperature and (b) in a magnified form at temperatures above 640K. Inspection shows these curves have many similarities to those obtained in other representative 7xxx-series alloys (for example, 7x50, 7449 and 7040 alloys) when treated to peak-aged (T6) and over-aged (T7) tempers [27]. Detailed research has revealed the primary thermal effects in these alloys [27,29] and these are labelled I to VI in Fig. 3a. In general terms, the major effects in these various regions are interpreted as Guinier-Preston (GP) zone and/or η′-phase dissolution (I), formation of the η-phase (II), coarsening of the η precipitates (III), dissolution of the η-phase (IV), incipient melting of the T-phase (V) and the onset of full melting of the alloy (VI). In addition, there may be other minor heating effects such as S-phase (Al_2CuMg) formation in alloys with high Cu and Mg contents and S-phase melting at an onset temperature of ~760K. The coarsening reaction designated as III involves the coarsening of η-phase rounded disks or spheres having diameters of ~10-50 nm [29].

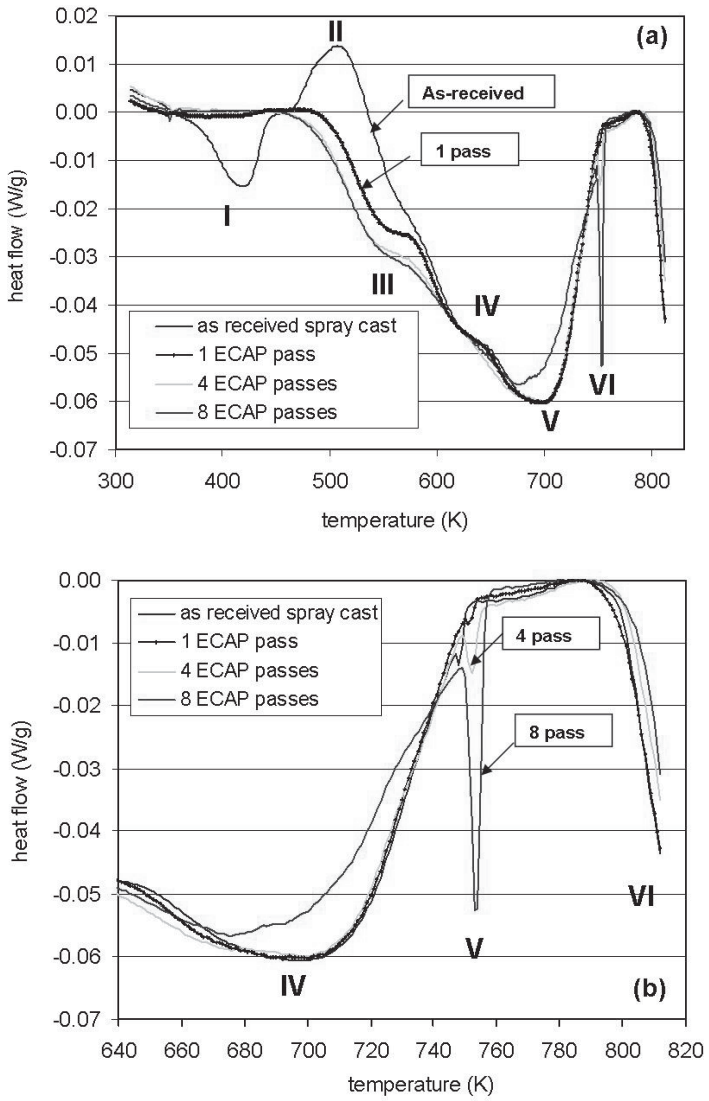

Fig. 3. The DSC curves obtained over a range of temperatures for the as-received material and after 1, 4 and 8 passes of ECAP: (a) overview and (b) magnified detail above a temperature of ~640K.

The DSC curve for the as-received alloy shown in Fig. 3 suggests that the η precipitation reaction starts initially on heating the billet to the ECAP temperature of 473K. For the samples subjected to ECAP, it is reasonable to anticipate that this reaction is largely completed during the first few ECAP passes, and the absence of effect II for the alloy subjected to 4 ECAP passes confirms this. Coarsening of the η-phase precipitates would occur on subsequent cycles of heating and passage through the ECAP die. The presence of these small η precipitates is evident in Fig. 2b and the occurrence of this precipitation at this temperature is consistent with results reported in other investigations of Al-Zn-Mg [35-37] and Al-Zn-Mg-Zr [38] alloys. It is important to recognize also that this precipitation reaction is especially favoured in samples subjected to ECAP processing because of the very high density of dislocations introduced into the grains during ECAP which stimulates η-phase formation by providing high diffusivity pathways and nucleation sites within the matrix [36]. In addition, the η-phase precipitates involved in reactions II and III in the DSC thermograms are distinct from the coarse rod-like η particles which are present in the as-received spray-cast material. However, these rod-like precipitates fragment in ECAP and they form the larger angular precipitates visible in Fig. 2b.

The DSC reactions I and II are typical precipitation and reversion reactions encountered in super-

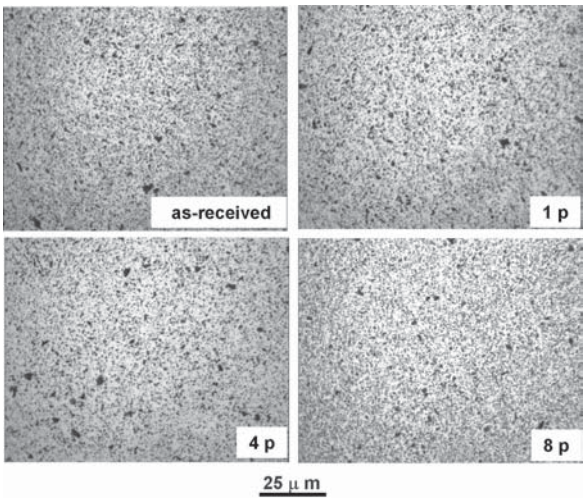

Fig. 4. Optical micrographs of the Al-7034 alloy (a) in the as-received condition and after (b) 1, (c) 4 and (d) 8 passes of ECAP.

saturated and under-aged Al-Zn-Mg(-Cu) alloys and they are the key to understanding the age-hardening characteristics. The coarser rod-like precipitates are not involved in these reactions and they have a relatively minor influence on precipitation strengthening. However, they play a significant role in pinning the grain boundaries and thereby restricting the occurrence of grain growth at elevated temperatures.

By comparing the DSC curves for the as-received condition and after ECAP through different numbers of passes in Fig. 3a, it is apparent that processing by ECAP at 473K leads to substantial precipitation of the η-phase with the consequent removal of reactions I and II even in the sample taken through only 1 pass. In addition, there is a very faint exothermic effect shown at III which is superimposed on a larger exothermic effect at approximately 530K: in practice, this effect is generally more pronounced for the peak-aged and slightly over-aged (T76 and T73-type) 7xxx-series alloys [26]. In the present samples, it is evident from Fig. 3a that this faint effect due to coarsening decreases with increasing numbers of ECAP passes, thereby demonstrating the occurrence of significant coarsening of the fine disk-shaped η precipitates during the ECAP passes to a state that is beyond the condition encountered in commercial T7 tempers.

Optical micrographs are shown in Fig. 4 for (a) the as-received alloy and the alloy after ECAP processing through (b) 1 pass, (c) 4 passes and (d) 8 passes. These micrographs reveal a reasonably homogeneous distribution of particles on the macroscopic scale with evidence for a wide range of particle sizes from ~3 μm down to the lower detection limit of ~0.2 μm. In general terms, the particle size distributions for the larger intermetallic particles seem to be reasonably unaffected by ECAP processing. However, a close comparison of Figs. 4a and 4b confirms that the rod-like precipitates with sizes close to ~0.5 μm in the as-received alloy are broken during ECAP and the more angular particles interspersed between the spherical precipitates appear to be the remnants of these rod-like precipitates. It is evident that ECAP processing at 473K causes two significant microstructural changes in addition to significantly refining the grain size. First, the rod-like η precipitates present in the as-received alloy with lengths of ~0.5 mm are fragmented by the high stresses imposed in ECAP. Second, fine η precipitates are formed and coarsen during the ECAP process and they reach sizes between ~10 and ~50 nm.

There is an addition interesting feature in the DSC curves in Fig. 3 because the trough in the h dissolution zone occurs close to ~700K in the as-received sample and in the samples subjected to 1 and 4 passes of ECAP whereas this trough is displaced to ~670K after 8 passes. The source of this displacement lies in the nature of the distributions and sizes of the fragmented η-phase particles after ECAP since any changes in these sizes and distributions will necessarily affect their rate of dissolution. It is reasonable to assume there is progressive breaking during ECAP so that pressing through 8 passes represents the most fragmented condition for the η-phase. This will alter dissolution and recrystallisation kinetics, and the combined effect is thought to be the cause of the altered dissolution effect.

The thermogram shown in Fig. 3b after 8 passes, and to a lesser extent the thermogram after 4 passes, reveals a clear melting of the T-phase at an onset temperature of approximately 750K. It is evident that the effective incipient melting temperature for the sample subjected to 8 passes of ECAP is reduced significantly from the value of 798K measured for the as-received material. The incipient melting of T phase also occurs in 7xxx-series aluminium alloys when the Mg content is in the range of 2-3% [39]. T-phase precipitation can occur at the ECAP temperature [40] but any precipitates formed during ECAP will be very small and are unlikely to be directly involved in the melting reaction appearing after several ECAP passes which is caused by the undissolved remnants of coarse particles.

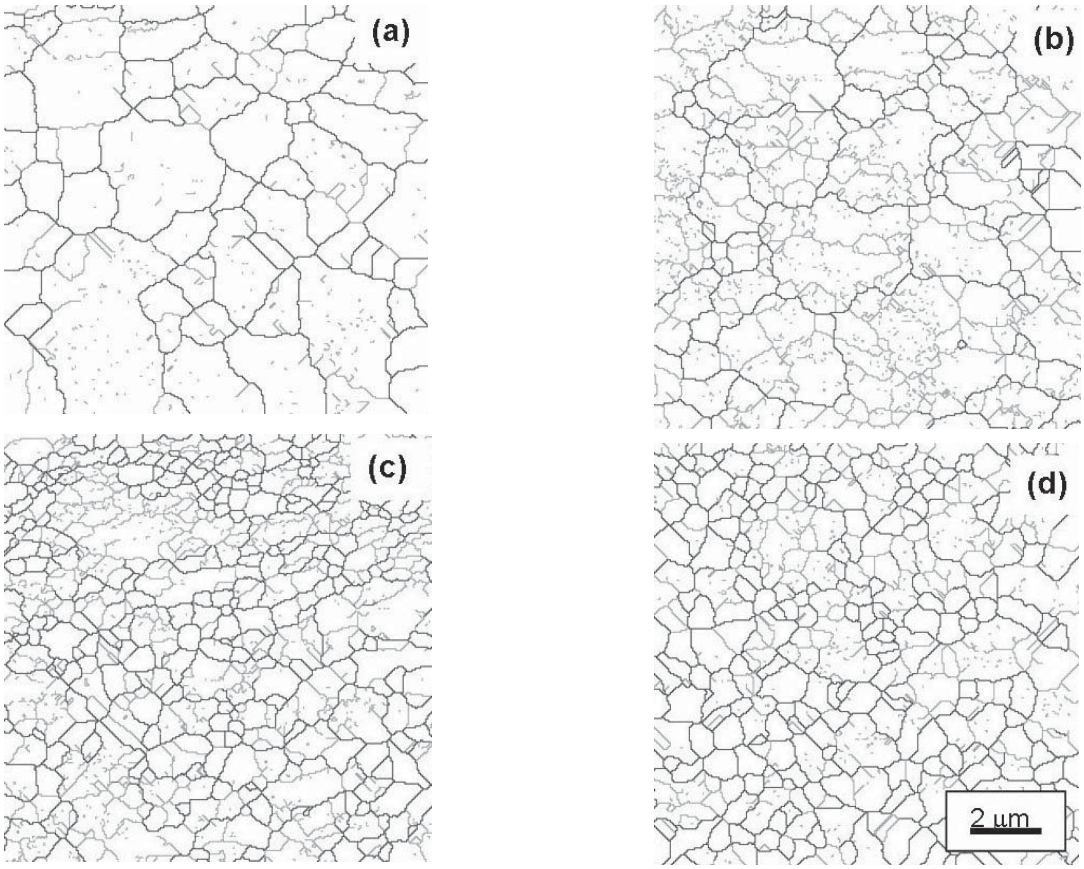

Fig. 5. Grain distributions in the Al-7034 alloy (a) in the as-received condition and after (b) 1, (c) 4 and (d) 8 passes of ECAP.

3.3. Grain morphology, grain boundary misorientations and texture

Typical grain boundary maps are shown in Fig. 5 for (a) the as-received material and after ECAP processing through (b) 1 pass, (c) 4 passes and (d) 8 passes: these maps were derived from a comprehensive EBSD analysis and the solid lines show the high-angle boundaries having measured misorientations ≥15°. A summary of the data derived from the EBSD analysis is given in Table 1 in terms of the average grain area, average grain diameter, the aspect ratio and the number of neighbouring grains.

For the as-received condition, the average grain size was determined from TEM as ~2.1 μm and this is broadly consistent with the EBSD measurements where the average grain size is ~1.7 μm. The small difference may be due in part to the choice of a lower cut-off misorientation angle which was set for the EBSD analysis at 2º. The average grain size of the alloy was reduced to ~0.6 μm in the first pass and to ~0.5 μm after 4 and 8 passes. By comparison, the average grain size after 8 passes was measured as ~0.3 μm by TEM. All of these results are generally consistent with the expectations for aluminium-based alloys [41]. The grain boundary maps shown in Fig. 5 provide a very clear demonstration of the changes taking place after pressing through 4 and 8 passes since, for both of these samples, the grain sizes are clearly much smaller than in the as-received condition or after 1 pass through the ECAP die. Thus, it is apparent that ECAP produces very significant grain refinement even in a spray-cast alloy where the initial grain size is extremely small.

The corresponding misorientation distributions are shown in Fig. 6 where the frequency of each angular increment is plotted in regular 3° increments and the solid curves correspond to the standard Mackenzie prediction for the distribution of misorientations in a randomly oriented polycrystal [42]. Three important conclusions may be reached

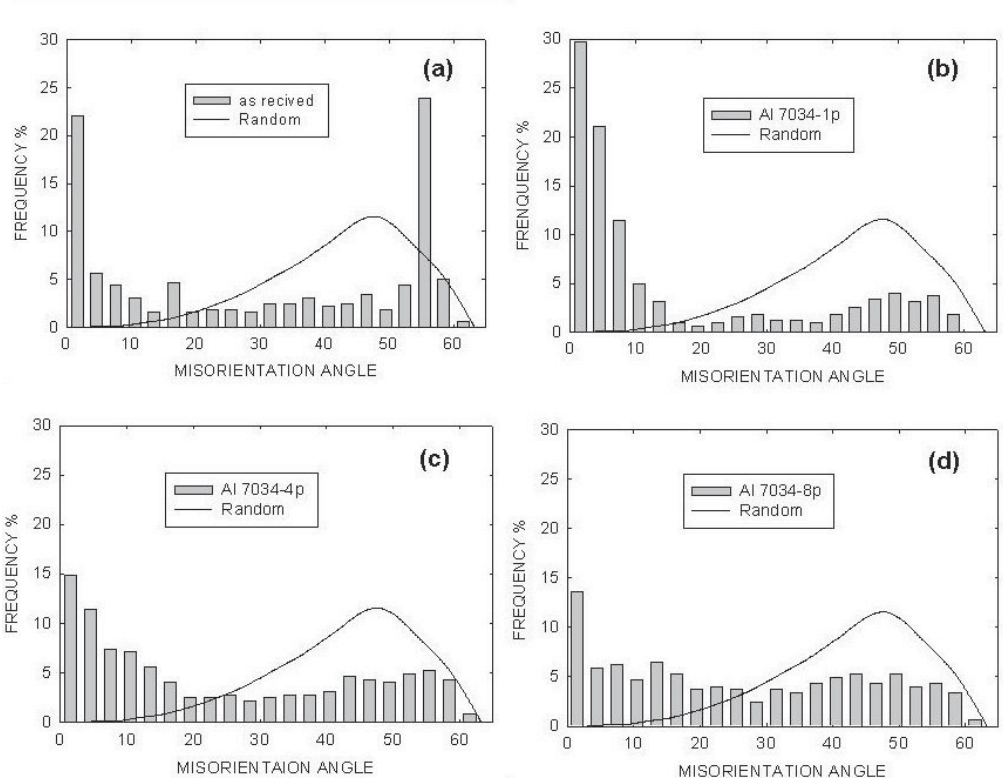

Fig. 6. Grain boundary misorientation distributions in the Al-7034 alloy (a) in the as-received condition and after (b) 1, (c) 4 and (d) 8 passes of ECAP.

through an examination of these histograms. First, the misorientation distribution for the as-received alloy shows the presence of a large fraction of low-angle boundaries but, in addition, there is an exceptionally large peak occurring at angles in the vicinity of ~55°. This peak is a genuine characteristic of the initial microstructure and it is a consequence of the presence of a very strong two fibre textures in the as-received material and the presence of a large fraction of Σ3 coincidence site lattice (CSL) boundaries. The presence of this fibre texture is demonstrated by the inverse pole figure for the as-received material shown as the upper plot in Fig. 7. It is interesting to note also that similar peaks have been reported in other materials such as an Fe-6.5% Si alloy [43] and nanocrystalline Ni fabricated by electrodeposition [44]. Second, a very high fraction of low-angle boundaries is present immediately after 1 pass of ECAP but thereafter the distribution becomes essentially bimodal with peaks at both high angles of misorientation in the vicinity of ~50° and at the lowest angles of <4º. Third, there is little or no difference between the distributions shown in Fig. 6 after 4 and 8 passes so that the angular distribution becomes fairly stabilized with an excess of low-angle boundaries. It is reasonable to conclude that the repetitive introduction of dislocations through each pass of ECAP leads to the continuous presence of low-angle boundaries in the microstructure thereby precluding the possibility of attaining a true Mackenzie distribution through ECAP. These results are consistent with the trends reported for pure aluminium and other aluminium-based alloys [45-48] and with other materials processed by ECAP such as Ni [49].

Fig. 7 shows the inverse pole figures for the as-received condition and after 1, 4 and 8 passes. These diagrams demonstrate a clear transition in the texture from an initial fibre $<111>_z$ and $<100>_z$ texture in the as-received condition to a $<101>_x$ texture after 1 pass, a $<111>_x$ texture after 4 passes and a $<100>_y$ texture after 8 passes.

Table 1. Microstructural characteristics of Al-7034 using EBSD analysis.

Condition	Grain area (μm^2)	Grain diameter (μm)	Aspect ratio	Number of neighbouring grains
As-received	2.79	1.66	1.57	5.67
1 pass	0.41	0.60	1.49	4.26
4 pass	0.26	0.49	1.63	5.26
8 pass	0.30	0.51	1.51	5.18

3.4. Mechanical properties and formability.

Tensile testing was conducted on both the as-received and the as-pressed alloy and the results are shown in Fig. 8 for tests conducted at temperatures from 573 to 673K and for pressed samples subjected to either 6 passes (6p) or 8 passes (8p) of ECAP. For the as-received and unpressed condition, the results shown in the upper plot of Fig. 8 reveal good ductility with elongations up to >500% at the highest testing temperature of 673K. These elongations are consistent with the exceptionally small grain size in the as-received condition. However, it is apparent from the lower plot in Fig. 8 that processing by ECAP introduces a significant enhancement in the ductilities such that the elongations to failure under optimum conditions increase

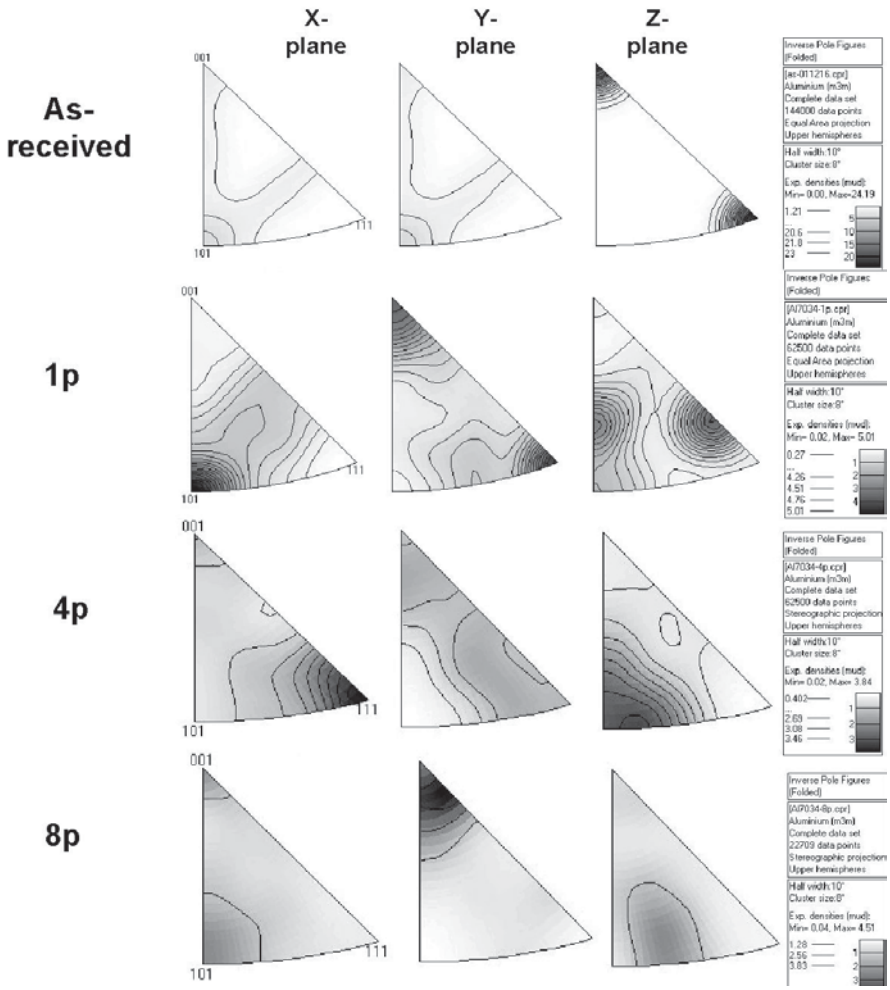

Fig. 7. Inverse pole figures for the Al-7034 alloy in the as-received condition and after 1 pass (second row), 4 passes (third row) and 8 passes (bottom row).

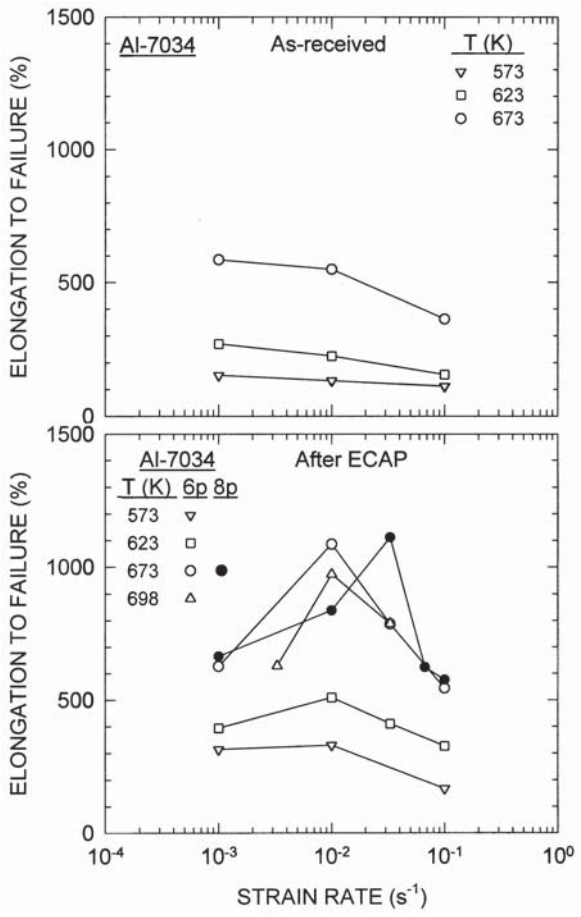

Fig. 8. Elongation to failure versus strain rate for the Al-7034 alloy in the as-received condition (upper) and for the alloy processed by ECAP for 6 and 8 passes (lower).

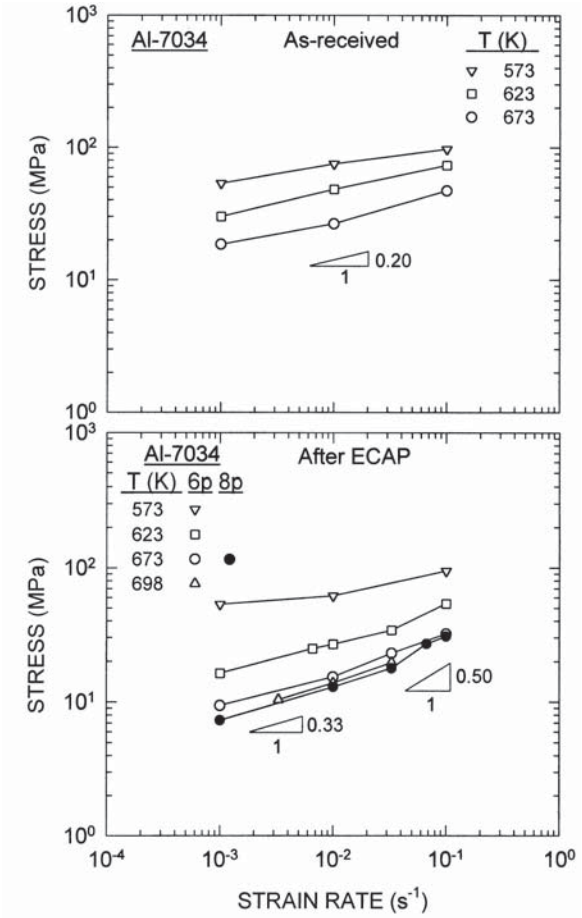

Fig. 9. Flow stress versus initial strain rate for the Al-7034 alloy in the as-received condition (upper) and for the alloy processed by ECAP for 6 and 8 passes (lower).

to >1000%. This increase is a direct consequence of the smaller grain size in the as-pressed alloy and the high fraction of high-angle grain boundaries that are conducive to easy grain boundary sliding.

Two important results are visible by close inspection of the plots in Fig. 8. First, whereas the elongations to failure increase with decreasing strain rate in the as-received condition, there is a sharp peak in the elongation at a strain rate ~10^{-2} s^{-1} in the pressed material after 6 passes of ECAP. The potential of achieving superplasticity at more rapid strain rates after ECAP was first suggested several years ago [16] and subsequently was confirmed in experiments on aluminium-based alloys [50]. Second, the pressed material exhibits exceptionally high elongations to failure by comparison with the as-received material and again this is anticipated because a detailed analysis has demonstrated the potential for high elongations at high strain rates as a natural consequence of the reduction in grain size inherent in ECAP processing [51]. The occurrence of a maximum elongation of ~1110% when testing at 673K after eight passes of ECAP is significant because this elongation was achieved at an initial strain rate of $3.3 \cdot 10^{-2}$ s^{-1} which is higher than the minimum strain rate of $1 \cdot 10^{-2}$ s^{-1} required in the formal definition of high strain rate superplasticity [52]. In addition, the slightly lower elongations achieved when testing at the higher temperature of 698K are probably due to the onset of grain growth and the difficulty of retaining ultrafine grain sizes at this very high temperature. The substantial dissolution of the η-phase precipitates on heating to 698K, as evident in the DSC thermogram in Fig. 3, reduces the number of grain boundary pinning particles and contrib-

utes to the increase in grain size at these high temperatures.

It is apparent also in Fig. 8 that the maximum elongation is displaced to a faster strain rate when the ECAP is taken through 8 passes instead of 6 passes. This trend is similar to earlier results for an Al-Mg-Li-Zr alloy [53] and it is a consequence of the increasing fraction of high-angle boundaries with increasing numbers of passes in ECAP [46]. High-angle boundaries are an important prerequisite for the occurrence of grain boundary sliding and superplastic flow so that an increase in the fraction of high-angle boundaries reduces the effective grain size and promotes the occurrence of superplasticity at faster strain rates.

Further information on the rate-controlling deformation mechanisms may be obtained by plotting the measured flow stress against the initial strain rate as shown in Fig. 9. For the as-received material, the strain rate sensitivity, m, is ~0.2 which is consistent with a dislocation climb process. For the material subjected to ECAP, there is a transition from a value of $m \approx 0.3$ at the lower strain rates to $m \approx 0.5$ at the higher strain rates corresponding to the region of optimum superplasticity. These values suggest a transition from control by a viscous glide process within the grains [54] to conventional superplasticity where the value of m is of the order of ~0.5 [55].

4. SUMMARY AND CONCLUSIONS

1. A spray-cast Al-7034 alloy, with an initial grain size of ~1.7 μm, was successfully processed by ECAP to reduce the grain size to ~0.3 μm. The as-received and the as-pressed materials were examined using a range of experimental techniques.
2. Processing by ECAP has two significant effects on the microstructure. There is a significant reduction in the grain size and the rod-like η-phase precipitates, initially having lengths of ~0.5 μm, are fragmented on each passage through the ECAP die.
3. An analysis by DSC reveals several important characteristics including the formation of η-phase and T-phase during ECAP processing, a dissolution of the η-phase at temperatures close to ~700K and a melting of the T-phase at temperatures close to ~750K.
4. The as-received alloy contains high fractions of both low-angle and high-angle boundaries and a large peak at angles in the vicinity of ~55° due to the presence of a fibre texture. Following ECAP, there is a bimodal distribution of boundary misorientations with a consistent high fraction of low-angle boundaries.
5. Superplastic elongations are attained in the material subjected to ECAP with elongations up to >1000% at a testing temperature of 673K. The strain rate sensitivity for the pressed material was measured as $m \approx 0.3$ but with a transition to $m \approx 0.5$ at the fastest strain rates where the elongations were a maximum.

ACKNOWLEDGEMENTS

This work was supported in part by the National Science Foundation of the United States under Grant No. DMR-0243331, in part by the Light Metals Educational Foundation of Japan and in part by INTAS under Project No. 03-51-3779. Dr S. Wang is acknowledged for assistance with analysis of EBSD data.

REFERENCES

[1] *Investigations and Applications of Severe Plastic Deformation*, ed. by T.C. Lowe and R.Z. Valiev (Kluwer Academic Publishers, Dordrecht, The Netherlands, 1999).
[2] R.Z. Valiev, R.K. Islamgaliev and I.V. Alexandrov // *Prog. Mater. Sci.* **45** (2000) 103.
[3] *Ultrafine Grained Materials II*, ed by Y.T. Zhu, T.G. Langdon, R.S. Mishra, S.L. Semiatin, M.J. Saran and T.C. Lowe (The Minerals, Metals and Materials Society, Warrendale, PA, 2002).
[4] *Nanomaterials by Severe Plastic Deformation*, ed by. M.J. Zehetbauer and R.Z. Valiev (Wiley VCH, Weinheim, Germany, 2004).
[5] *Ultrafine Grained Materials III*, ed. by Y.T. Zhu, T.G. Langdon, R.Z. Valiev, S.L. Semiatin, D.H. Shin and T.C. Lowe (The Minerals, Metals and Materials Society, Warrendale, PA, 2004).
[6] Z. Horita, T. Fujinami and T.G. Langdon // *Mater. Sci. Eng.* **A318** (2001) 34.
[7] V.M. Segal, V.I. Reznikov, A.E. Drobyshevskiy and V.I. Kopylov // *Metally* **1** (1981) 115.
[8] V.M. Segal, V.I. Reznikov, V.I. Kopylov, D.A. Pavlik and V.F. Malyshev, *Process of Structure Formation during Plastic Straining* (Scientific and Technical Publishing, Minsk, Belarus, 1994).
[9] V.M. Segal // *Mater. Sci. Eng.* **A197** (1995) 157.
[10] V.M. Segal // *Mater. Sci. Eng.* **A271** (1999) 322.

[11] M. Furukawa, Z. Horita, M. Nemoto and T.G. Langdon // *J. Mater. Sci.* **36** (2001) 2835.
[12] R.Z. Valiev, N.A. Krasilnikov and N.K. Tsenev // *Mater. Sci. Eng.* **A137** (1991) 35.
[13] R.Z. Valiev, A.V. Korznikov and R.R. Mulyukov // *Mater. Sci. Eng.* **A168** (1993) 141.
[14] E.O. Hall // *Proc. Roy. Soc. B* **64** (1951) 747.
[15] N.J. Petch // *J. Iron Steel Inst.* **174** (1953) 25.
[16] Y. Ma, M. Furukawa, Z. Horita, M. Nemoto, R.Z. Valiev and T.G. Langdon // *Mater. Trans. JIM* **37** (1996) 336.
[17] M. Furukawa, Y. Iwahashi, Z. Horita, M. Nemoto, N.K. Tsenev, R.Z. Valiev and T.G. Langdon // *Acta Mater.* **45** (1997) 4751.
[18] H. Hasegawa, S. Komura, A. Utsunomiya, Z. Horita, M. Furukawa, M. Nemoto and T.G. Langdon // *Mater. Sci. Eng.* **A265** (1999) 188.
[19] M. Furukawa, A. Utsunomiya, K. Matsubara, Z. Horita and T.G. Langdon // *Acta Mater.* **49** (2001) 3829.
[20] S. Lee, A. Utsunomiya, H. Akamatsu, K. Neishi, M. Furukawa, Z. Horita and T.G. Langdon // *Acta Mater.* **50** (2002) 553.
[21] S. Lee, M. Furukawa, Z. Horita and T.G. Langdon // *Mater. Sci. Eng.* **A342** (2003) 294.
[22] A. Gholinia and P.B. Prangnell // *Mater. Sci. Tech.* **15** (1999) 328.
[23] Z.C. Wang and P.B. Prangnell // *Mater. Sci. Eng.* **A328** (2002) 87.
[24] C. Xu, W. Dixon, M. Furukawa, Z. Horita and T.G. Langdon // *Mater. Lett.* **57** (2003) 3588.
[25] C. Xu, M. Furukawa, Z. Horita and T.G. Langdon // *Acta Mater.* **51** (2003) 6139.
[26] N. Gao, L. Davin, S. Wang, A. Cerezo and M.J. Starink // *Mater. Sci. Forum* **395-402** (2002) 923.
[27] M.J. Starink and X.M. Li // *Metall. Mater. Trans.* **34A** (2003) 899.
[28] J.A. Wert // *Scripta Mater.* **15** (1981) 445.
[29] M.J. Starink and S.C. Wang // *Acta Mater.* **51** (2003) 5131.
[30] Y. Iwahashi, J. Wang, Z. Horita, M. Nemoto and T.G. Langdon // *Scripta Mater.* **35** (1996) 143.
[31] M. Furukawa, Y. Iwahashi, Z. Horita, M. Nemoto and T.G. Langdon // *Mater. Sci. Eng*. **A257** (1998) 328.
[32] M. Murayama, Z. Horita and K. Hono // *Acta Mater.* **49** (2001) 21.
[33] K. Oh-ishi, Y. Hashi, A. Sadakata, K. Kaneko, Z. Horita and T.G. Langdon // *Mater. Sci. Forum* **396-402** (2002) 333.
[34] C.Y. Nam, J.H. Han, Y.H. Chung and M.C. Shin // *Mater. Sci. Eng.* **A347** (2003) 255.
[35] R.M. Allen and J.B. Vande Sande // *Metall. Mater. Trans.* **9A** (1978) 1251.
[36] R.M. Allen and J.B. Vande Sande // *Acta Metall.* **28** (1980) 1185.
[37] K. Stiller, P.J. Warren, V. Hansen, J. Angenete and J. Gjénnes // *Mater. Sci. Eng.* **A270** (1999) 55.
[38] V. Hansen, O.B. Karlsen, Y. Langsrud and J. Gjénnes // *Mater. Sci. Tech.* **20** (2004) 185.
[39] X. Li and M.J. Starink // *Mater. Sci. Forum* **331-337** (2000) 1071.
[40] A. Deschamps, F. Livet and Y. Bréchet // *Acta Mater.* **47** (1999) 281.
[41] Y. Iwahashi, Z. Horita, M. Nemoto and T.G. Langdon // *Metall. Mater. Trans*. **29A** (1998) 2503.
[42] J.K. Mackenzie // *Biometrika* **45** (1958) 229.
[43] T. Watanabe // *Textures and Microstructures* **20** (1993) 195.
[44] K. Harada, S. Tsurekawa, T. Watanabe and G. Palumbo // *Scripta Mater.* **49** (2003) 367.
[45] J.-Y. Chang, J.-S. Yoon and G.-H. Kim // *Scripta Mater.* **45** (2001) 347.
[46] S.D. Terhune, D.L. Swisher, K. Oh-ishi, Z. Horita, T.G. Langdon and T.R. McNelley // *Metall. Mater. Trans.* **33A** (2002) 2173.
[47] P.L. Sun, C.Y. Yu, P.W. Kao and C.P. Chang // *Scripta Mater.* **47** (2002) 377.
[48] P.-L. Sun, P.-W. Kao and C.-P. Chang // *Metall. Mater. Trans.* **35A** (2004) 1359.
[49] A.P. Zhilyaev, B.-K. Kim, G.V. Nurislamova, M.D. Baró, J.A. Szpunar and T.G. Langdon // *Scripta Mater.* **46** (2002) 575.
[50] R.Z. Valiev, D.A. Salimonenko, N.K. Tsenev, P.B. Berbon and T.G. Langdon // *Scripta Mater.* **37** (1997) 1945.
[51] C. Xu, M. Furukawa, Z. Horita and T.G. Langdon // *Adv. Eng. Mater.* **5** (2003) 359.
[52] K. Higashi, M.Mabuchi and T.G. Langdon // *ISIJ Intl.* **36** (1996) 1423.
[53] S. Lee, P.B. Berbon, M. Furukawa, Z. Horita, M. Nemoto, N.K. Tsenev, R.Z. Valiev and T.G. Langdon // *Mater. Sci. Eng.* **A272** (1999) 63.
[54] F.A. Mohamed and T.G. Langdon // *Acta Metall.* **22** (1974) 779.
[55] T.G. Langdon // *Acta Metall. Mater.* **42** (1994) 2437.